Journal of the American Society for
Mass Spectrometry

pubs.acs.org/jasms Volume 31, Issue 5 May 2020

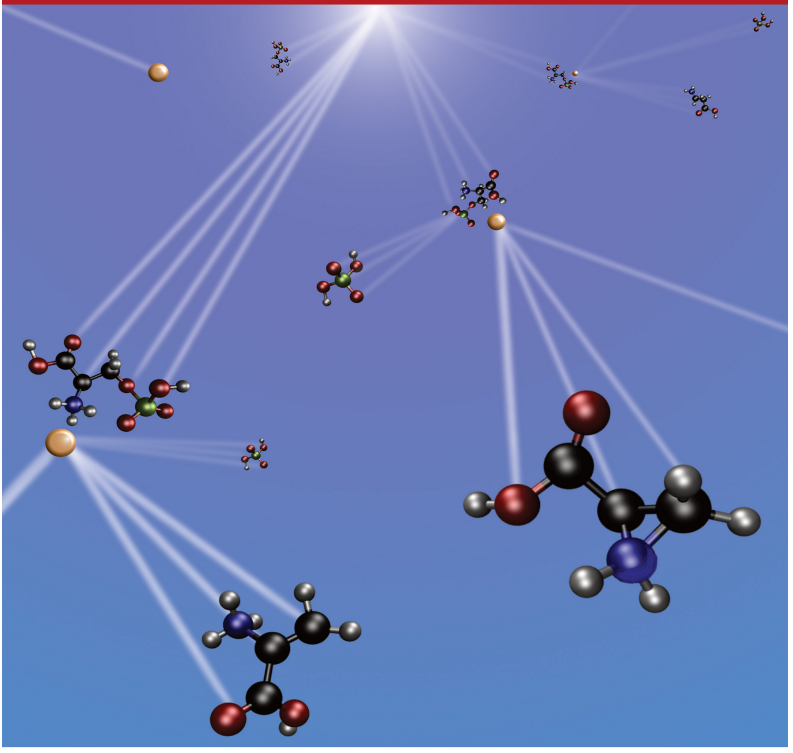

ACS Publications
Most Trusted. Most Cited. Most Read.

www.asms.org www.acs.org

PUBLISHED IN PARTNERSHIP WITH ASMS AND ACS PUBLICATIONS

ACS Partner Journal

Journal of the American Society for Mass Spectrometry

pubs.acs.org/jasms

Research Article

Modeling the Effects of *O*-Sulfonation on the CID of Serine

Kenneth Lucas and George L. Barnes*

Cite This: *J. Am. Soc. Mass Spectrom.* 2020, 31, 1114−1122

Read Online

ACCESS | Metrics & More | Article Recommendations | Supporting Information

ABSTRACT: We present the results of direct dynamics simulations and DFT calculations aimed at elucidating the effect of *O*-sulfonation on the collision-induced dissociation for serine. Toward this end, direct dynamics simulations of both serine and sulfoserine were performed at multiple collision energies and theoretical mass spectra obtained. Comparisons to experimental results are favorable for both systems. Peaks related to the sulfo group are identified and the reaction dynamics explored. In particular, three significant peaks (m/z 106, 88, and 81) seen in the theoretical mass spectrum directly related to the sulfo group are analyzed as well as major peaks shared by both systems. Our analysis shows that the m/z 106 peaks result from intramolecular rearrangements, intermolecular proton transfer among complexes composed of initial fragmentation products, and at high energy side-chain fragmentation. The m/z 88 peak was found to contain multiple constitutional isomers, including a previously unconsidered, low energy structure. It was also observed that the RM1 semiempirical method was not able to obtain all of the major peaks seen in experimens for sulfoserine. In contrast, PM6 did obtain all major experimental peaks.

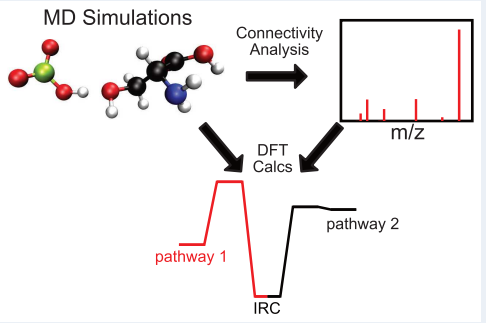

1. INTRODUCTION

Significant experimental[1−5] and theoretical[6−8] work has been performed to examine both the chemical and physical aspects of MS2 systems. It is known that the addition of post-translational modifications (PTM) can expand the functional diversity of proteins and peptides by altering their configurational space,[9] enzymatic efficiency,[10] signaling properties,[11] and a myriad of other biochemically important criteria.[12] Such PTMs can occur at the N-terminus, C-terminus, side chain, or backbone depending on the modification and the residue. The phosphate modification, particularly *O*-phosphorylation of threonine and serine, is ubiquitous and has long been studied.[13,14] However, the sulfate analogue was only recently first described in the literature in 2004,[15] and as such, much less work has been done on peptide sulfonation, especially within the realm of proteomics, though some initial work has been performed.[16,17]

Recently, Polfer and co-workers have studied the MS2 spectra of *O*-sulfonated serine (sulfoserine - m/z 186) through both collision-induced dissociation (CID) mass spectrometry and infrared multiple photon dissociation (IRMPD) spectroscopy.[18] The CID measurements found that there were two major fragmentation pathways, one associated with SO_3 loss (m/z 106) and one associated with H_2SO_4 loss (m/z 88). In addition, DFT calculations were used along with the IRMPD spectra to infer product structures. Proposed mechanisms were also provided based on chemical intuition.

Molecular dynamics (MD) simulations have been previously used to investigate the fragmentation pathways of unmodified amino acids and peptides and are known to yield results in reasonable agreement with experiment.[6−8] Performing MD simulations of gas phase amino acids and peptides has lent valuable insight into the complicated, short-time scale fragmentation dynamics taking place during CID, which often follow unexpected reaction pathways. The calculation of an ensemble of trajectories that simulate random collisions of the ion species of interest and the subsequent dynamics allows for a guided approach to the investigation of the fragmentation mechanisms via ab initio calculations. Hence, it is expected that a direct dynamics/DFT study would provide insight into the sulfoserine system.

In this work, we will investigate both the serine and sulfoserine system using a quantum mechanical (QM) + molecular mechanical (MM) direct dynamics approach followed by high-level DFT calculations to accurately quantify the relevant stationary points along the most important reaction pathways. This will allow for an evaluation of the effect of PTM on the reaction dynamics as well as a comparison of our short-time results to the long-time results of Polfer.

An outline for the remainder of the paper is as follows: in section 2, we provide an overview of our computational method; in section 3, we present our results and discuss what

Received: February 3, 2020
Revised: March 23, 2020
Accepted: March 23, 2020
Published: March 23, 2020

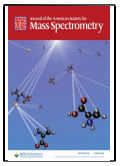

https://dx.doi.org/10.1021/jasms.0c00037
J. Am. Soc. Mass Spectrom. 2020, 31, 1114−1122

insight our calculations provide regarding the reaction dynamics; and in section 4, we provide a summary.

2. COMPUTATIONAL METHODS

The use of direct dynamics simulations to investigate MS2 systems has been well described in the literature,[6,7,19] and hence, only a summary is provided here. The interested reader is directed to the recent tutorial review which describes the computational approach to surface-induced dissociation[7] and an Account & Perspective published in this journal on CID.[6] This approach is aimed at modeling the dynamics of experiments in which the kinetic energy of the collision is well-known and controlled, such as threshold collision-induced dissociation.[20] Experimental setups in which the resulting internal energy distribution is Maxwell−Boltzmann[21] can also be modeled via thermal excitation. Preliminary simulations found similar results between the two methods; however, the thermal simulations produced a greater number of minor peaks. Hence, we choose to perform simulations with a controlled initial collision energy as they appear to more closely mirror the experimental results. Below, we will describe our treatment of the potential energy function used for the dynamics simulations, how the starting structure for sulfoserine was obtained, and an overview of the initial conditions. Our analysis method is then described.

2.1. Potential Energy. Following the established method, we write our potential energy function for the collision system as a sum of intramolecular and intermolecular terms. Specifically, the potential energy is given by

$$V = V_{\text{peptide}} + V_{\text{Ar}-\text{peptide}} \tag{1}$$

where V_{peptide} is the intramolecular potential of the peptide (serine or sulfoserine) and $V_{\text{Ar}-\text{peptide}}$ is the intermolecular potential. In this work, we choose to use semiempirical methods to calculate V_{peptide}. In particular, we investigated both RM1 and PM6 initially. RM1 has been shown to provide good results in simulations;[19,22−27] however, we found that it lacked some important mass peaks that PM6 was able to obtain. A similar deficiency was seen in the recent simulations of Macaluso et al.[28] in which it was found that PM6-D outperformed RM1. To our knowledge, these are the only two direct dynamics simulations that have employed RM1 for systems containing sulfo groups, and both works concluded that a version of PM6 was superior. Given that it is now known that RM1 is deficient for sulfo-containing species, we will focus our discussion on the PM6 results and provide some analogous RM1 results in the Supporting Information.

The intermolecular potential, $V_{\text{Ar}-\text{peptide}}$, is calculated as the sum of two-body Buckingham potential terms between argon and the atoms in the amino acid, expressed as

$$V_{\text{Ar}-\text{peptide}} = A_{\text{Ar-}k} e^{-B_{\text{Ar-}k} R_{Ar-k}} + \frac{C_{\text{Ar-}k}}{R^9_{\text{Ar-}k}} \tag{2}$$

where the index k represents an atom within the amino acid and $R_{\text{Ar}-k}$ is the interatomic distance. The parameters for the intermolecular interactions with C, N, O and H were developed by Meroueh and Hase,[29] while those for the terms involving the SO_4 moiety were parametrized by Oritz et al.[30] These parameters result in an intermolecular potential that is strictly repulsive, which is sufficient for our simulations.

2.2. Structures and Simulation Method. We generated initial structures using Avogadro[31] followed by optimization from Mopac2016.[32] Once optimized, the peptide was given a random orientation about its center of mass along with a 300 K vibrational and rotational distribution using normal mode sampling.[33] The impact parameter was randomly chosen between 0 and 3 Å, and the argon atom was situated 20 Å from the center of mass of the molecule, which ensures no initial interaction. A total of 1500 trajectories were calculated for each collision energy between 2.00 and 11.00 at 1.50 eV increments. This type of simulation methodology results in translational to internal energy transfer. The distributions of internal energy for the ion after the collision are provided in the Supporting Information. We solved Hamiltonian equations of motion for each trajectory using a 6th order symplectic integration scheme[34] for total simulation time of 50 ps with a 1 fs step size and output written every 50 fs. This was accomplished via an in-house simulation package coupled with Mopac2012.[35] Following the collision, argon was removed when the MM interaction $V_{\text{Ar}-\text{peptide}}$ fell below 1×10^{-3} kcal/mol. In addition, since only charged fragments are observed in experiments, neutral fragments were removed from the simulation if they were at least 15 Å away from any charged fragments. To accomplish this, we expanded on the approach of Barnes et al.[36] for automatic identification of fragmentation products. That approach makes use of a bond order matrix calculated on-the-fly using the semiempirical Hamiltonian. The solution of the semiempirical Hamiltonian also yields partial atomic charges, and hence, charged fragments can be identified. The distance between neutral fragments and any charged fragment within the system was checked every picosecond. Once neutral fragments were identified, a QM energy calculation was performed before and after removal. The difference between these calculations was tracked so that energy conservation could still be tested. The removal of neutral fragments improved the computational efficiency and self-consistent field convergence. Preliminary simulations also revealed that for the serine/sulfoserine system, secondary fragmentation did not occur for charged species with $m/z \leq 60$. Hence, simulations were terminated if the charged fragment was below this cutoff. Moreover, experimental observation of low mass products can be problematic and ultimately our goal is to provide information relevant to experiment. Energy was well conserved for all trajectories.

2.3. Theoretical Mass Spectra and Reaction Pathways. Our in-house simulation package calculates bond orders between all QM atoms for all steps within the simulation. With this information, both the connectivity and the number of fragments is available for each simulation step. This in turn allows for theoretical mass spectra to be automatically constructed for both species as well as providing data for a group theory analysis of the products that contribute to each peak.[37,38] With this knowledge of the final products, as well as the intermediates, we generated structures that are close to the minima, intermediates, and transition states of interest and proceeded to optimize them at the ωB97X-D/aug-cc-pVTZ level of theory using Gaussian09 software.[39]

3. RESULTS AND DISCUSSION

3.1. Serine Mass Spectrum. We begin our discussion by examining the results for the comparatively simple serine system. The theoretical mass spectrum for serine at a collision energy of 8 eV is displayed in Figure 1, and it is seen that the spectrum is dominated by the m/z 60 peak at all collision energies considered. This peak corresponds to the loss of H_2O

https://dx.doi.org/10.1021/jasms.0c00037
J. Am. Soc. Mass Spectrom. 2020, 31, 1114−1122

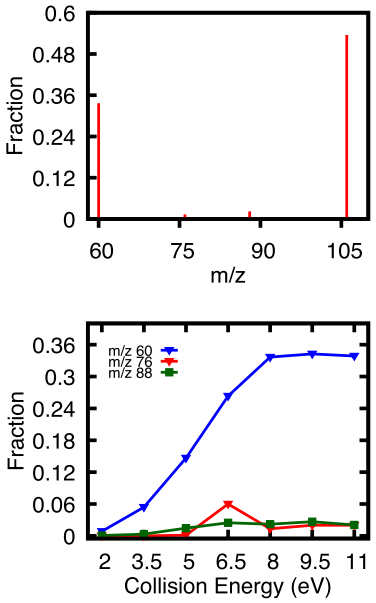

Figure 1. Example theoretical mass spectrum obtained from a collision energy of 8 eV for serine along with the collision energy dependence of the major product peaks. It is seen that at this collision energy and within the time frame of the simulation, the majority of trajectories do not dissociate. The most significant dissociation peak occurs at m/z 60, which corresponds to H_2O + CO or $C(OH)_2$ loss. Fractions are relative to the total number of trajectories calculated.

+ CO or $C(OH)_2$. Roughly 55% yield the first product at 8 eV. The m/z 60 pathway is produced via two mechanisms: (1) loss of water occurring at the C-terminus as a result of a proton hop from the N-terminus and shortly thereafter loss of CO from the C-terminus and (2) loss of $C(OH)_2$ occurs via a proton hop to the carbonyl oxygen from the N-terminus that results in the C-terminus dissociating. Initial attempts to optimize the transition states associated with the loss of the C-terminus were unsuccessful largely due to the locally shallow PES. We also observe the m/z 88 peak, which is associated with the loss of water and occurs through three different mechanisms. Water is lost during the first step for one of the mechanisms for the formation of m/z 60, and hence, m/z 88 is an intermediate. It is likely that with additional simulation time, such intermediates would react to m/z 60 as well. The next two mechanisms are similar and result in the formation of m/z 88 due to a proton migration to the alcohol of the side chain followed by water dissociation. The source of the proton is either the N-terminus or the α carbon. There is one additional minor peak, m/z 76, which corresponds to loss of the side chain without proton migration occurring. Recently, Zhang et al.[40] studied the fragmentation of 19 amino acids using high-resolution electrospray ionization MS/MS, and found previously unreported fragmentation products for several systems. Their experimental serine spectra shows three peaks, namely m/z 88, 70, 60. At all collision energies considered by Zhang, m/z 60 was the dominant pathway with m/z 88 showing a decrease with collision energy (see Figure S37 and S38 of that work). Our theoretical results are in good qualitative agreement with the work of Zhang et al.[40] though we do not see the m/z 70 peak, which is attributed to the loss of two waters. It is reasonable to assume that the second water loss occurs on a time scale longer than our simulation time. It is likely that the two mechanisms that result in the m/z 88 pathway via water loss from the side chain could lead to a second water loss via the C-terminus due to proton migration from either the α carbon or the N-terminus depending on the source of the proton for the initial water loss.

3.2. Sulfoserine Mass Spectrum. Turning our attention to sulfoserine, the theoretical mass spectrum at a collision energy of 8 eV along with the collision energy dependence of the major product peaks is shown in Figure 2. The four most

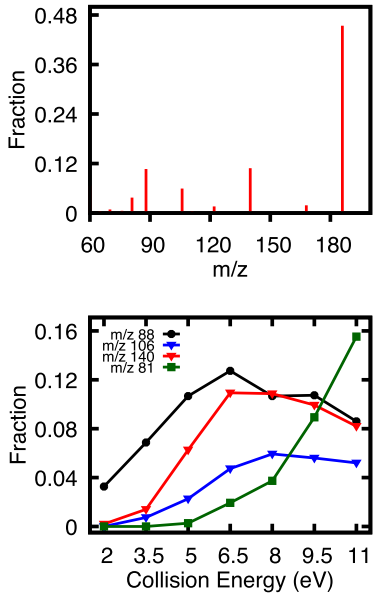

Figure 2. Example theoretical mass spectrum obtained from a collision energy of 8 eV along with the collision energy dependence of the major product peaks. It is seen that at this collision energy and within the time frame of the simulation, the majority of trajectories do not dissociate. The most significant dissociation peaks are m/z 140, 106, 88, and 81. m/z 81 is seen to dramatically increase in intensity at large collision energies. The m/z 88 and 106 peaks are the dominant peaks seen in experimental CID work of Polfer and co-workers. Fractions are relative to the total number of trajectories calculated.

significant peaks are m/z 140, 106, 88, and 81 which correspond to loss of H_2O + CO or $C(OH)_2$, loss of SO_3, loss of H_2SO_4, and formation of HSO_3^+, respectively. These results are in good qualitative agreement with the CID experiments of Polfer and co-workers[18] with the exception that m/z 129 was not observed in our spectrum and m/z 81 was not observed in the experiment. The m/z 129 is a minor peak that was not analyzed in this or the experimental work, while m/z 81 grows in intensity with collision energy in our simulations and will be discussed below. Of the four peaks observed (140, 106, 88, and 81) in our simulations, the last three peaks all involve the PTM, while the first follows an equivalent mechanism as that seen in unmodified serine: loss of either H_2O + CO or $C(OH)_2$. The former occurs 65% of the time, making it slightly more probable than in unmodified serine.

3.2.1. Sulfoserine m/z 106. Connectivity analysis of the trajectories yielding the m/z 106 fragment ion was performed and revealed that protonated serine is the dominant species in the peak. This agrees with previous experimental CID work by Polfer and co-workers.[18] However, that work only proposed one mechanism for the m/z 106 pathway, whereas multiple mechanisms were observed in the simulations for the m/z 106 pathway. Moreover, there are three different classes of

https://dx.doi.org/10.1021/jasms.0c00037
J. Am. Soc. Mass Spectrom. 2020, 31, 1114−1122

Scheme 1. Mechanisms for *m/z* 106 Pathway

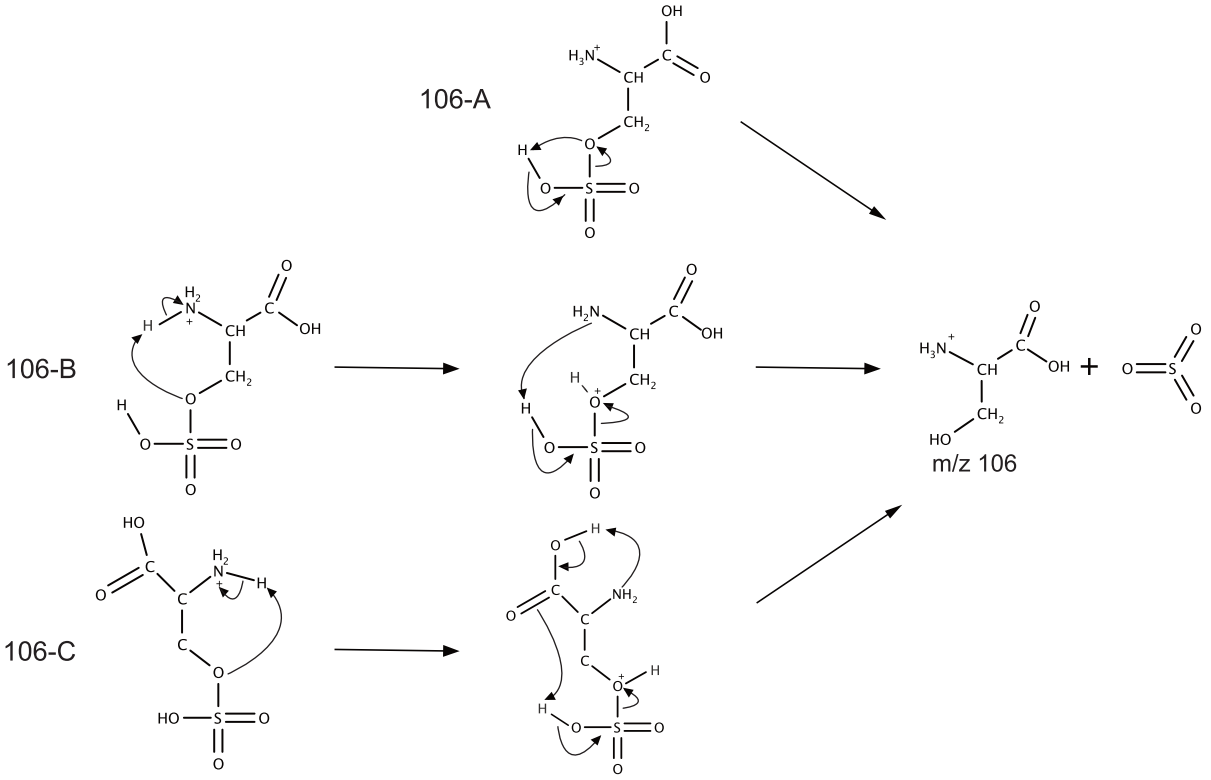

mechanisms that can form the *m/z* 106 peak: (1) intramolecular rearrangement reactions, such as those shown in Scheme 1, (2) intermolecular proton transfer reactions that take place due to complexation of fragmentation products, and (3) "shattering" mechanisms that are rare and only occur at large collision energies. As an aside, we note that the theoretical spectrum resulting from simulations using RM1 did not contain the *m/z* 106 peak, and hence, the method was deemed insufficient for this system. Since *m/z* 106 results from cleavage of the S−O bond, it can be assumed that RM1 overestimates such bond strengths.

The first class of mechanisms are shown schematically in Scheme 1. Polfer and co-workers proposed Mechanism 106-A, which produces SO_3 from sulfoserine in a concerted step by transferring the sulfate proton to the linker oxygen of the side chain. In our simulations, this mechanism dominates the *m/z* 106 peak for all collision energies. The lowest fraction of occurrence for the mechanism is 0.66 at a collision energy of 8 eV, whereas the largest fraction is one relative to the total population of the *m/z* 106 peak. DFT calculations estimate that the barrier for this reaction is 38.1 kcal/mol and involves the migration of a single proton. While this mechanism is dominant, there are other intramolecular rearrangements that can occur. In particular, it is possible for the excess proton on the N-terminus to become involved as shown in Mechanism 106-B: a proton transfer occurs from the N-terminus to the side chain oxygen followed by a transfer from the sulfate group back to the N-terminus, releasing SO_3 and generating N-protonated serine. This mechanism can take place in two different ways, depending on the conformation present. If the conformation has a short N to O distance, then there is no energy minimum corresponding to the first step. This single well character is similar to that seen in low barrier hydrogen bonds (also called short strong hydrogen bonds),[41] a class of hydrogen bond that have been found to be important for proton transfer in biological systems.[42] As such, the first proton transfer can take place along the intrinsic reaction coordinate (IRC) toward the transition state for the second mechanistic step. Although this transition state emphasizes motion of the second proton, some displacement in position of both protons is seen. If the N to O distance is large when transfer occurs, then 106-B takes place with two distinct transition states, though the potential landscape is still relatively flat with a shallow minimum defining the intermediate. At a collision energy of 8 eV, the fraction of *m/z* 106 that results from Mechanism 106-B is 0.079. DFT calculations show that this mechanism has a barrier of 44.1 kcal/mol and involves the migration of two protons.

The carbonyl oxygen of the C-terminus can also be involved in the generation of the protonated serine ion, though it is much less common. Mechanism 106-C involves proton transfers from the N-terminus to the oxygen of the side chain and from the sulfate group to the carbonyl oxygen. This step is followed by a transfer from the C-terminus to the N-terminus to generate N-protonated serine and SO_3. DFT calculations show that these three proton transfer reactions occur along an IRC that involves motion of all three protons and has a barrier of 29.9 kcal/mol. Mechanism 106-C is not observed for most collision energies but does account for 0.014 of *m/z* 106 at a collision energy of 6.5 eV. Its lack of prevalence in the simulations is likely due to the large number of protons that need to be exchanged, and hence depends sensitively on the overall conformation of the system.

The second class of mechanism involves intermolecular proton transfer reactions that are reminiscent of the ion-neutral complexes known in mass spectrometry[43,44] and is dynamically similar to atom roaming mechanisms.[45] These mechanisms typically include the same first step as 106-B and C, namely a

https://dx.doi.org/10.1021/jasms.0c00037
J. Am. Soc. Mass Spectrom. 2020, 31, 1114−1122

Scheme 2. Mechanisms for *m/z* 88 Pathway

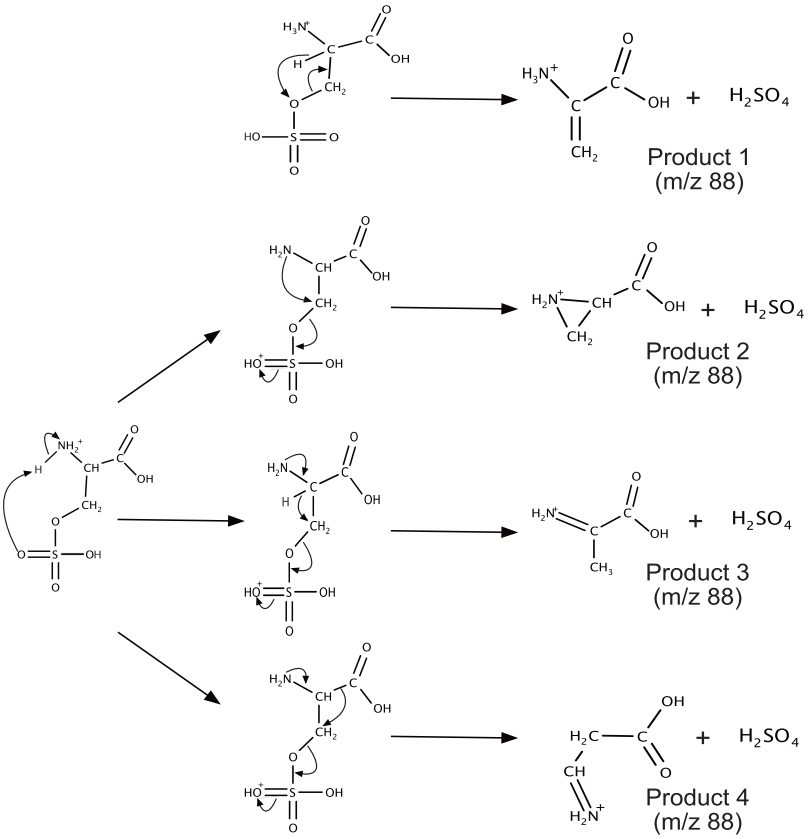

proton transfer from the N-terminus to the linking oxygen. This transfer results in the formation of HSO_3^+ along with neutral serine. A complex then forms between the charged and neutral fragmentation products. The formation of such complexes between fragmentation products in simulations has previously been studied by Barnes and co-workers[26] for the octaglycine system. In that system, it was found that complexes could be very long-lived and allow for unique final products. In this system, the complexes can be long-lived or fleeting, depending on the proton motion taking place in the rest of the system along with the conformation of the system when the S−O bond cleaves. The final *m/z* 106 product is generated by the transfer of the proton from HSO_3^+ to serine. Multiple different acceptor sites have been observed, though it is common for the proton to transfer to the side-chain alcohol, which simultaneously transfers the proton that was already at that location back to the N-terminus. A similar type of mechanism has been observed at the C-terminus; transfer occurs to the carbonyl oxygen along with a simultaneous transfer of the acidic proton back to the N-terminus. This class of mechanism is significant and has a maximum contribution to *m/z* 106 of 0.265 at a collision energy of 5 eV.

The final class for *m/z* 106 is shattering mechanisms, which are both rare and only occur at large collision energies. As such only qualitative comments can be made. This class of reaction mechanism produces *m/z* 106, but not protonated serine. Rather, these trajectories result in the loss of multiple small molecules and one charged cyclic product, namely H_2O + CO + c((S═O)OCH_2CHN^+H) with the S atom within the 5-member ring structure.

3.2.2. Sulfoserine m/z 88. We performed the same connectivity analysis to determine the structure of the *m/z* 88 fragment ion. However, unlike the majority of the products for the *m/z* 106 ion pathway, the *m/z* 88 pathway was observed to consist of several different constitutional isomers. In fact, 11 different products were identified for this peak. These products were efficiently sorted and quantified by using the connectivity information collected during the trajectory combined with group theoretical analysis—it is known that the lowest eigenvalue of the weighted adjacency matrix uniquely determines the particular constitutional isomer.[37,38] Of the possible product ions, all but three are minor products within our simulation. The mechanisms for the formation of these products is given in Scheme 2 and their relative contribution to the *m/z* 88 peak is shown in Figure 3. Many of the other eight structures are seen at large collision energies and result from backbone rearrangement reactions.

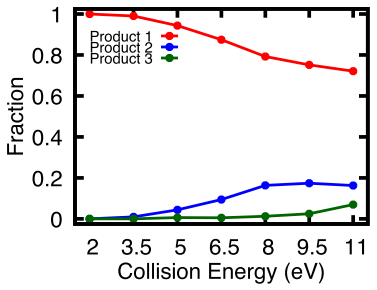

Figure 3. Time evolution for the distribution of products observed within the *m/z* 88 peak. While Product 1 is dominant throughout the entire collision energy range, it is seen to decrease with collision energy as competition from other products increases. Fractions are relative to the total population with *m/z* 88.

https://dx.doi.org/10.1021/jasms.0c00037
J. Am. Soc. Mass Spectrom. 2020, 31, 1114−1122

Product 1 is seen to be most important in the simulations for all collision energies, starting at a fraction relative to the total population of m/z 88 of 1 for 2 eV and moving down to ~0.75 at 11 eV with products 2 and 3 increasing to 0.17 and 0.07, respectively. Polfer and co-workers proposed five different possible structures for m/z 88 that occur either via direct loss of H_2SO_4 or loss of SO_3 followed by loss of H_2O. The proposed products included our product 1 and 2, but not 3; we observed three of the five proposed structures. In contrast to Polfer, who assigned product 2 to be the most likely structure based on IRMPD measurements/DFT calculations, we observed product 1 as most important in our short time simulations. This may be due to the short time scale of the simulations or that PM6 underestimates the reaction barrier for this process.

A schematic overview of the reaction mechanisms for the m/z 88 pathway is provided in Figure 4 with energies provided for both the DFT and PM6 calculations. We note that the trends observed in Figure 3 follow the relative energetics of the PM6 transition states. We also note that the DFT energetics are both qualitatively and quantitatively different for some of these transition states. This highlights the importance of performing higher level calculations, when possible, following semi-empirical direct dynamics simulations. Although the semi-empirical calculations are quite close for several of the structures, if it had been computationally feasible for the dynamics to be performed with DFT and a triple-ζ basis set, Figure 3 would likely have shown product 2 to dominate at low collision energies.

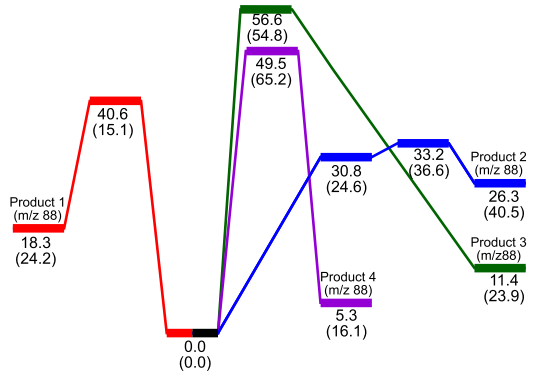

Figure 4. Schematic overview of the energy landscape for products 1−4 along with the energy, in kcal/mol, of the relevant minima, intermediates, products, and transition states at the ωB97X-D/aug-cc-pVTZ and PM6 (in parentheses) level of theories.

The mechanism for the formation of product 1 follows a direct, one-step process to release H_2SO_4 via loss of the α carbon's hydrogen atom. This mechanism is slightly different than that proposed by Polfer in that the linking oxygen to the sulfo group is not involved. Product 2 is generated from a two-step mechanism involving an intermediate that results from a proton transfer from the N-terminus to the sulfate group. In the global minima, the proton that is transferred is hydrogen bonded to the sulfate group, but in the intermediate, following the transfer, this proton is stabilized by a hydrogen bond to the C-terminus carbonyl group. There is no barrier for a return to the global minima, and hence the system readily reverts. This reversibility and the underestimate of product 1's barrier likely accounts for the populations observed in the simulations. Product 3, which also involves a proton transfer from the N-terminus to the sulfo group, forms directly from the global minima, does not pass through the stabilized intermediate observed for product 2, and increases with collision energy monotonically. This is consistent with product 3's higher barrier but more stable final structure. The reaction barriers at the PM6 level of theory for both products 2 and 3 are within 3 kcal/mol of the DFT values. The DFT calculations for products 1−3 also yielded the mechanism for product 4. While product 4 is observed in the simulations, it is not a major product. However, on the basis of the DFT calculations, it could be important. The PM6 barrier for this TS is 65.2 kcal/mol, which is 15.7 kcal/mol higher than in the DFT calculations, which could explain why it is not often seen in the PM6 simulations. While the mechanism involves a proton transfer from the N-terminus to the sulfate group, it proceeds directly to products.

The experimental assignment of the m/z 88 ion as product 2 two was based on IRMPD measurements compared to DFT frequency calculations.[18] In addition, the product resulting from loss of phosphoric acid from phosphoserine has also been identified as 2-carboxyaziridine via both traditional MS methods[13] and IRMPD measurements.[14] However, the DFT calculations here suggest that our product 4 could also be important. To provide a complete data set for all possible products, we decided to closely compare the theoretical IR spectra for each ion. Katari et al.[46] have recently shown that use of a linear correlation rather than a simple scaling improves mean absolute error for experimental vs scaled frequencies and, in particular, focused on comparison to IRMPD data. Hence, we reoptimized structures for products 1−4 using the B3LYP/6-31+G(d,p) level of theory and obtained their vibrational frequencies. Katari found that this choice of functional and basis set produced the best results. Lorentzian line shapes with 30 cm^{-1} fwhm were applied to each and presented in Figure 5 along with lines showing the centers of the most important experimental IRMPD peaks as identified by Polfer and co-workers. We note that the full experimental spectrum is available in Figure 4 of Polfer and co-workers.[18] Product 2 is likely the better match to the observed IRMPD spectrum; however, the two are fairly close and it is notable that product 4 does not have a peak at ~3200 cm^{-1}, but rather one at ~2988 cm^{-1}, which is out of the experimentally observable range. Product 2 has the lowest energy intrinsinc reaction coordinate, whereas product 4 is the most thermodynamically stable. Thus, it is plausible that either could dominate depending on the experimental conditions.

3.2.3. Sulfoserine m/z 81. The m/z 81 peak is seen to dramatically increase as the other three ion intensities slowly taper. While this CID peak was not observed by Polfer and co-workers, it is possible that it was not present at the collision energy considered in that experiment. The m/z 81 peak corresponds to the formation of HSO_3^+. One obvious source for this peak has already been discussed; a lack of proton transfer from HSO_3^+ back to serine which results in m/z 81 rather than m/z 106. Hence, proton transfer is acting as a "decision maker" between m/z 106 and 81 in a similar way as observed for the OH^- ion in the work of Macaluso et al.[28] At a collision energy of 11 eV, this mechanism accounts for a 0.53 fraction of the m/z 81 peak. However, this is not the sole source of m/z 81. Another major mechanism, with a 0.35 fraction of the peak, is the complete loss of the side-chain. The side-chain itself then fragments to form HSO_3^+ + CH_2O, without any proton transfer occurring between the initial fragmentation products.

https://dx.doi.org/10.1021/jasms.0c00037
J. Am. Soc. Mass Spectrom. 2020, 31, 1114−1122

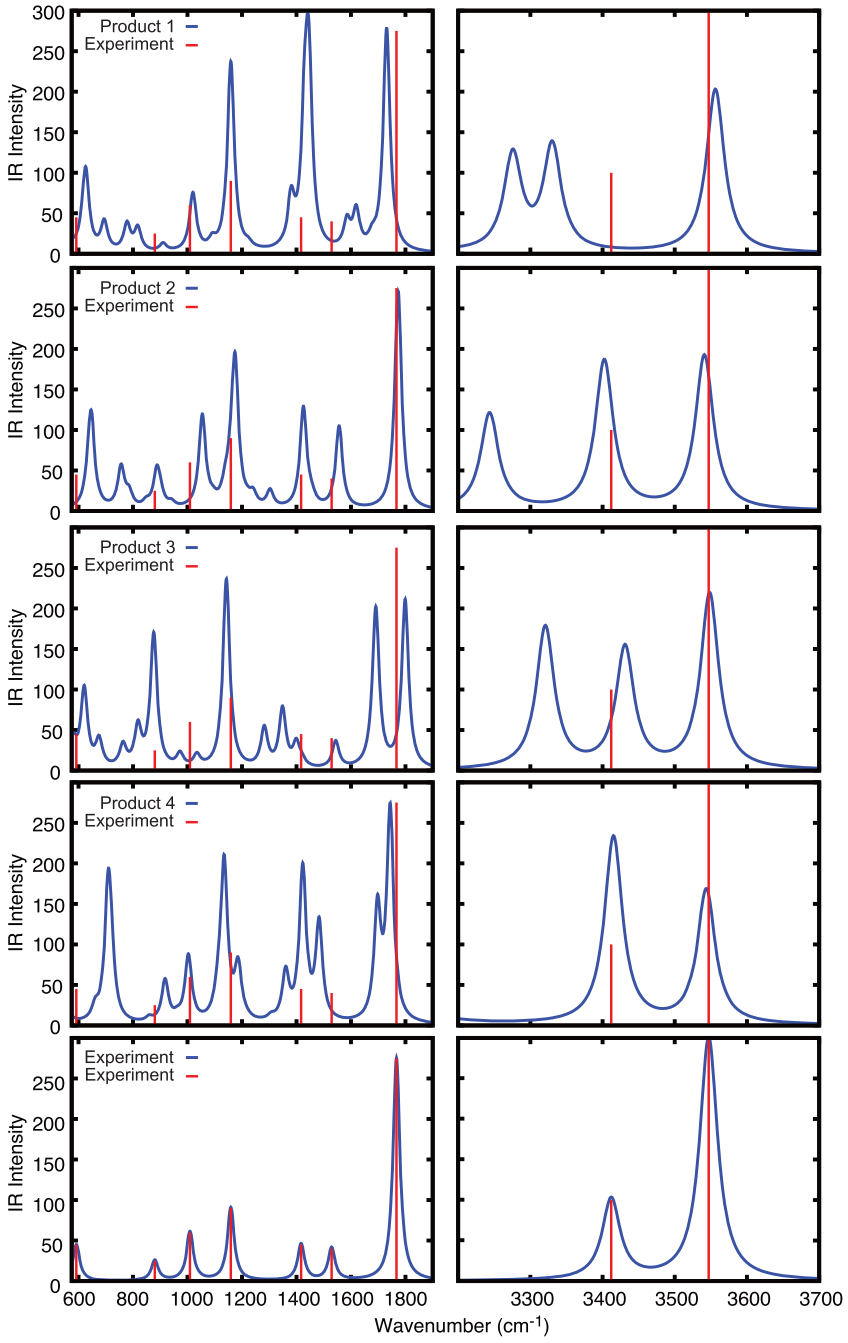

Figure 5. Comparison of the DFT frequencies for Products 1−4 in the m/z 88 pathway along with the major experimental IRMPD peaks identified by Polfer and co-workers. Experimental intensities are estimated, while theoretical peaks are obtained from a linear correlation correction. DFT spectra are represented using a 30 cm^{-1} fwhm Lorentzian line shape. Experimental data is shown as both a line spectra as well as with a 30 cm^{-1} fwhm Lorentzian line shape.

The fragments of the side chain often complex; however, for this peak, that complex is broken without charge transfer occurring. The next most favored mechanism, with a 0.05 fraction of the peak, follows the same steps with the addition of water loss occurring at what was the C-terminus. The remaining components of the peak are distributed among eight other minor products.

4. SUMMARY

We have presented results from direct dynamics simulations and DFT calculations that highlighted the differences between unmodified serine and sulfoserine. In general, the direct dynamics simulations show good qualitative agreement with the experimental work of Zhang et al. (serine)[40] as well as Polfer and co-workers (sulfoserine).[18] Transition state searches, geometry optimizations, and IRC calculations were performed to elucidate the potential energy surface for sulfoserine based on the products observed from the dynamics simulations.

The major peaks observed in the sulfoserine experiment were m/z 106 and 88. Detailed analysis was performed on these peaks. The m/z 106 pathway was found to be formed through three different classes of mechanism: intramolecular rearrangement, intermolecular proton transfer reactions, and

https://dx.doi.org/10.1021/jasms.0c00037
J. Am. Soc. Mass Spectrom. 2020, 31, 1114−1122

"shattering" processes. The dominant mechanism involves a direct, one-step mechanism that was also put forward by Polfer and co-workers. Our work highlights that other rearrangement mechanisms are possible, but in addition, intermolecular mechanisms involving proton transfer from initial fragmentation products were observed as a significant mechanism for this peak.

The composition of the m/z 88 pathway was analyzed and compared to the findings of Polfer and co-workers. The dynamics simulations show that Product 1 is the favored isomer for all collision energies and times considered; however, this is likely due to the underestimation of the reaction barrier by PM6. Product 2, which was identified by Polfer as the dominant species, was seen to increase with collision energy. DFT calculations also show that, based on energetics, product 4 may also be important, although it is a minor mechanism in simulations due to the overestimation of this reaction barrier by PM6 compared to the DFT results. The other barriers for m/z 88 were well reproduced by PM6. The mechanism that forms product 2 has the lowest reaction barriers, while product 4 is the most thermodynamically stable. A detailed comparison of the vibrational frequencies is provided for both of these products. While product 2 is likely a better match for the experimental IRMPD measurements of Polfer, the two species share many spectral features.

The m/z 81 feature is observed in simulations, but not in the experimental work. This may be due to the energy at which the experiment was conducted. The m/z 81 and 106 peaks are in fact linked in that the intermolecular proton transfer mechanisms that produce m/z 106 could also result in m/z 81 if the complex breaks before proton transfer occurs. This is consistent with m/z 81 being more prevalent at high collision energies. In addition, m/z 81 arises through side-chain loss followed by fragmentation of the side-chain itself, which is again a high energy process.

■ ASSOCIATED CONTENT

Supporting Information

The Supporting Information is available free of charge at https://pubs.acs.org/doi/10.1021/jasms.0c00037.

RM1 results analogous to Figure 2; example change in internal energy distribution and average/standard deviations for (1) the change in internal energy, (2) change in vibrational energy, and (3) change in rotational energy for sulfoserine (PDF)

■ AUTHOR INFORMATION

Corresponding Author

George L. Barnes − *Department of Chemistry and Biochemistry, Siena College, Loudonville, New York 12211, United States;* orcid.org/0000-0001-9211-2736; Email: gbarnes@siena.edu

Author

Kenneth Lucas − *Department of Chemistry and Biochemistry, Siena College, Loudonville, New York 12211, United States*

Complete contact information is available at: https://pubs.acs.org/10.1021/jasms.0c00037

Notes

The authors declare no competing financial interest.

■ ACKNOWLEDGMENTS

G.L.B. and K.L. gratefully acknowledge support from the National Science Foundation under grant No. 1763652. Dr. K. Kolonko is thanked for insightful conversations.

■ REFERENCES

(1) Cooks, R. G.; Ast, T.; Pradeep, T.; Wysocki, V. H. Reactions of Ions with Organic Surfaces. *Acc. Chem. Res.* **1994**, *27*, 316−323.

(2) Ouyang, Z.; Takáts, Z.; Blake, T. A.; Gologan, B.; Guymon, A. J.; Wiseman, J. M.; Oliver, J. C.; Davisson, V. J.; Cooks, R. G. Preparing Protein Microarrays by Soft-Landing of Mass-Selected Ions. *Science* **2003**, *301*, 1351−1354.

(3) Laskin, J.; Denisov, E.; Futrell, J. H. A Comparative Study of Collision-Induced and Surface-Induced Dissociation. 1. Fragmentation of Protonated Dialanine. *J. Am. Chem. Soc.* **2000**, *122*, 9703−9714.

(4) Laskin, J.; Wang, P.; Hadjar, O. Soft-Landing of Peptide Ions Onto Self-Assembled Monolayer Surfaces: An Overview. *Phys. Chem. Chem. Phys.* **2008**, *10*, 1079−1090.

(5) Wang, P.; Hadjar, O.; Gassman, P. L.; Laskin, J. Reactive Landing of Peptide Ions on Self-Assembled Monolayer Surfaces: An Alternative Approach for Covalent Immobilization of Peptides on Surfaces. *Phys. Chem. Chem. Phys.* **2008**, *10*, 1512−1522.

(6) Martin Somer, A.; Macaluso, V.; Barnes, G. L.; Yang, L.; Pratihar, S.; Song, K.; Hase, W. L.; Spezia, R. Role of Chemical Dynamics Simulations in Mass Spectrometry Studies of Collision-Induced Dissociation and Collisions of Biological Ions with Organic Surfaces. *J. Am. Soc. Mass Spectrom.* **2020**, *31*, 2−24.

(7) Pratihar, S.; Barnes, G. L.; Hase, W. L.; Pratihara, S.; Barnes, G. L.; Hase, W. L. Chemical Dynamics Simulations of Energy Transfer, Surface-Induced Dissociation, Soft-Landing, and Reactive- Landing in Collisions of Protonated Peptide Ions with Organic Surfaces. *Chem. Soc. Rev.* **2016**, *45*, 3595−3608.

(8) Pratihar, S.; Barnes, G. L.; Laskin, J.; Hase, W. L. Dynamics of Protonated Peptide Ion Collisions with Organic Surfaces. Consonance of Simulation and Experiment. *J. Phys. Chem. Lett.* **2016**, *7*, 3142−3150.

(9) Kumar, A.; Narayanan, V.; Sekhar, A. Characterizing Post-Translational Modifications and Their Effects on Protein Conformation Using NMR Spectroscopy. *Biochemistry* **2020**, *59*, 57−73.

(10) Ryšlavá, H.; Doubnerová, V.; Kavan, D.; Vaněk, O. Effect of posttranslational modifications on enzyme function and assembly. *J. Proteomics* **2013**, *92*, 80−109.

(11) Boscher, C.; Dennis, J. W.; Nabi, I. R. Glycosylation, galectins and cellular signaling. *Curr. Opin. Cell Biol.* **2011**, *23*, 383−392.

(12) Karve, T. M.; Cheema, A. K. Small Changes Huge Impact: The Role of Protein Posttranslational Modifications in Cellular Homeostasis and Disease. *J. Amino Acids* **2011**, *2011*, 207691.

(13) Reid, G. E.; Simpson, R. J.; O'Hair, R. A. Leaving group and gas phase neighboring group effects in the side chain losses from protonated serine and its derivatives. *J. Am. Soc. Mass Spectrom.* **2000**, *11*, 1047−1060.

(14) Lanucara, F.; Chiavarino, B.; Scuderi, D.; Maitre, P.; Fornarini, S.; Crestoni, M. E. Kinetic control in the CID-induced elimination of H_3PO_4 from phosphorylated serine probed using IRMPD spectroscopy. *Chem. Commun.* **2014**, *50*, 3845−3848.

(15) Medzihradszky, K. F.; Darula, Z.; Perlson, E.; Fainzilber, M.; Chalkley, R. J.; Ball, H.; Greenbaum, D.; Bogyo, M.; Tyson, D. R.; Bradshaw, R. A.; Burlingame, A. L. O-sulfonation of serine and threonine. *Mol. Cell. Proteomics* **2004**, *3*, 429−443.

(16) Seibert, C.; Sakmar, T. P. Toward a framework for sulfoproteomics: Synthesis and characterization of sulfotyrosine-containing peptides. *Biopolymers* **2008**, *90*, 459−477.

(17) Huang, B. Y.; Chen, P. C.; Chen, B. H.; Wang, C. C.; Liu, H. F.; Chen, Y. Z.; Chen, C. S.; Yang, Y. S. High-Throughput Screening of Sulfated Proteins by Using a Genome-Wide Proteome Microarray and Protein Tyrosine Sulfation System. *Anal. Chem.* **2017**, *89*, 3278−3284.

(18) Patrick, A. L.; Stedwell, C. N.; Schindler, B.; Compagnon, I.; Berden, G.; Oomens, J.; Polfer, N. C. Insights into the fragmentation pathways of gas-phase protonated sulfoserine. *Int. J. Mass Spectrom.* **2015**, *379*, 26.
(19) Barnes, G. L.; Hase, W. L. Energy Transfer, Unfolding, and Fragmentation Dynamics in Collisions of N-Protonated Cctaglycine with an H-SAM Surface. *J. Am. Chem. Soc.* **2009**, *131*, 17185−17193.
(20) Rodgers, M. T.; Ervin, K. M.; Armentrout, P. B. Statistical modeling of collision-induced dissociation thresholds. *J. Chem. Phys.* **1997**, *106*, 4499−4508.
(21) Shukla, A. K.; Futrell, J. H. Tandem mass spectrometry: Dissociation of ions by collisional activation. *J. Mass Spectrom.* **2000**, *35*, 1069−1090.
(22) Frederickson, D.; McDonough, M.; Barnes, G. L. A Computational Comparison of Soft Landing of Alpha-Helical vs Globular Peptides. *J. Phys. Chem. B* **2018**, *122*, 9549−9554.
(23) Barnes, G. L.; Podczerwinski, A. Simulating the Effect of Charge State on Reactive Landing of a Cyclic Tetrapeptide on Chemically Modified Alkylthiolate Self-Assembled Monolayer Surfaces. *J. Phys. Chem. C* **2017**, *121*, 14628−14635.
(24) Shaikh, K.; Blackwood, J.; Barnes, G. L. The Effect of Protonation Site and Conformation on Surface-Induced Dissociation in a Small, Lysine Containing Peptide. *Chem. Phys. Lett.* **2015**, *637*, 83−87.
(25) Gregg, Z.; Ijaz, W.; Jannetti, S.; Barnes, G. L. The Role of Proton Transfer in Surface-Induced Dissociation. *J. Phys. Chem. C* **2014**, *118*, 22149−22155.
(26) Ijaz, W.; Gregg, Z.; Barnes, G. L. Complex Formation during SID and Its Effect on Proton Mobility. *J. Phys. Chem. Lett.* **2013**, *4*, 3935−3939.
(27) Geragotelis, A.; Barnes, G. L. Surface Deposition Resulting from Collisions Between Diglycine and Chemically Modified Alkylthiolate Self-Assembled Monolayer Surfaces. *J. Phys. Chem. C* **2013**, *117*, 13087−13093.
(28) Macaluso, V.; Scuderi, D.; Crestoni, M. E.; Fornarini, S.; Corinti, D.; Dalloz, E.; Martinez-Nunez, E.; Hase, W. L.; Spezia, R. L -Cysteine Modified by S-Sulfation: Consequence on Fragmentation Processes Elucidated by Tandem Mass Spectrometry and Chemical Dynamics Simulations. *J. Phys. Chem. A* **2019**, *123*, 3685−3696.
(29) Meroueh, O.; Hase, W. L. Collisional Activation of Small Peptides. *J. Phys. Chem. A* **1999**, *103*, 3981−3990.
(30) Ortiz, D.; Salpin, J.-Y.; Song, K.; Spezia, R. Galactose-6-Sulfate collision-induced dissociation using QM+MM chemical dynamics simulations and ESI-MS/MS experiments. *Int. J. Mass Spectrom.* **2014**, *358*, 25−35.
(31) Hanwell, M. D.; Curtis, D. E.; Lonie, D. C.; Vandermeersch, T.; Zurek, E.; Hutchison, G. R. Avogadro: An Advanced Semantic Chemical Editor, Visualization, and Analysis Platform. *J. Cheminf.* **2012**, *4*, 17.
(32) Stewart, J. P. Mopac2016, 2016; http://openmopac.net.
(33) Peslherbe, G. H.; Wang, H.; Hase, W. L. Monte Carlo Sampling for Classical Trajectory Simulations. *Adv. Chem. Phys.* **2007**, *105*, 171−201.
(34) Schlier, C.; Seiter, A. High-Order Symplectic Integration: An Assessment. *Comput. Phys. Commun.* **2000**, *130*, 176−189.
(35) Stewart, J. P. Mopac2012, 2012; http://openmopac.net.
(36) Barnes, G. L.; Young, K.; Yang, L.; Hase, W. L. Fragmentation and Reactivity in Collisions of Protonated Diglycine with Chemically Modified Perfluorinated Alkylthiolate-Self-Assembled Monolayer Surfaces. *J. Chem. Phys.* **2011**, *134*, 094106.
(37) Vázquez, S. A.; Otero, X. L.; Martinez-Nunez, E. A trajectory-based method to explore reaction mechanisms. *Molecules* **2018**, *23*, 3156.
(38) Rodríguez, A.; Rodríguez-Fernández, R.; Vázquez, S. A.; Barnes, G. L.; Stewart, J. P.; Martínez-Núñez, E. tsscds2018: A code for automated discovery of chemical reaction mechanisms and solving the kinetics. *J. Comput. Chem.* **2018**, *39*, 1922−1930.
(39) Frisch, M. J.; Trucks, G. W.; Schlegel, H. B.; Scuseria, G. E.; Robb, M. A.; Cheeseman, J. R.; Scalmani, G.; Barone, V.; Mennucci, B.; Petersson, G. A.; Nakatsuji, H.; Caricato, M.; Li, X.; Hratchian, H. P.; Izmaylov, A. F.; Bloino, J.; Zheng, G.; Sonnenberg, J. L.; Hada, M.; Ehara, M.; Toyota, K.; Fukuda, R.; Hasegawa, J.; Ishida, M.; Nakajima, T.; Honda, Y.; Kitao, O.; Nakai, H.; Vreven, T.; Montgomery, J. A., Jr.; Peralta, J. E.; Ogliaro, F.; Bearpark, M.; Heyd, J. J.; Brothers, E.; Kudin, K. N.; Staroverov, V. N.; Kobayashi, R.; Normand, J.; Raghavachari, K.; Rendell, A.; Burant, J. C.; Iyengar, S. S.; Tomasi, J.; Cossi, M.; Rega, N.; Millam, N. J.; Klene, M.; Knox, J. E.; Cross, J. B.; Bakken, V.; Adamo, C.; Jaramillo, J.; Gomperts, R.; Stratmann, R. E.; Yazyev, O.; Austin, A. J.; Cammi, R.; Pomelli, C.; Ochterski, J. W.; Martin, R. L.; Morokuma, K.; Zakrzewski, V. G.; Voth, G. A.; Salvador, P.; Dannenberg, J. J.; Dapprich, S.; Daniels, A. D.; Farkas, Ö.; Foresman, J. B.; Ortiz, J. V.; Cioslowski, J.; Fox, D. J. *Gaussian 09*, Revision D.01. 2009.
(40) Zhang, P.; Chan, W.; Ang, I. L.; Wei, R.; Lam, M. M.; Lei, K. M.; Poon, T. C. Revisiting Fragmentation Reactions of Protonated α-Amino Acids by High-Resolution Electrospray Ionization Tandem Mass Spectrometry with Collision-Induced Dissociation. *Sci. Rep.* **2019**, *9*, 6453.
(41) Humbel, S. Short strong hydrogen bonds: A valence bond analysis. *J. Phys. Chem. A* **2002**, *106*, 5517−5520.
(42) Vishveshwara, S.; Madhusudhan, M. S.; Maizel, J. V. Short-strong hydrogen bonds and a low barrier transition state for the proton transfer reaction in RNase A catalysis: A quantum chemical study. *Biophys. Chem.* **2001**, *89*, 105−117.
(43) McAdoo, D. J. Ion-neutral complexes in unimolecular decompositions. *Mass Spectrom. Rev.* **1988**, *7*, 363−393.
(44) Longevialle, P. Ion−neutral complexes in the unimolecular reactivity of organic cations in the gas phase. *Mass Spectrom. Rev.* **1992**, *11*, 157−192.
(45) Suits, A. G. Roaming atoms and radicals: A new mechanism in molecular dissociation. *Acc. Chem. Res.* **2008**, *41*, 873−881.
(46) Katari, M.; Nicol, E.; Steinmetz, V.; van der Rest, G.; Carmichael, D.; Frison, G. Improved Infrared Spectra Prediction by DFT from a New Experimental Database. *Chem. - Eur. J.* **2017**, *23*, 8414−8423.

https://dx.doi.org/10.1021/jasms.0c00037
J. Am. Soc. Mass Spectrom. 2020, 31, 1114−1122